

Distinguishing Majorana bound states from Andreev bound states through differential conductance and current noise spectrum

Huajin Zhao,¹ Junrong Wang,¹ Hong Mao,^{1,*} and Jinshuang Jin^{1,†}

¹*School of Physics, Hangzhou Normal University, Hangzhou, Zhejiang 311121, China*

(Dated: February 11, 2025)

We investigate the quantum transport through a quantum dot coupled with a superconducting (SC) nanowire. By elaborating the differential conductance and current noise spectrum, we focus on the distinct characteristics of the topological Majorana bound states (MBSs) and trivial Andreev bound states (ABSs) hosted in SC wire. For MBSs with a topological quality factor $q = 1$, we observe the degenerate features manifested as the zero-bias peak (ZBP) in differential conductance and the Rabi dips degeneracy (RDD) in noise spectrum. In contrast, for ABSs with $q < 1$, the splitting of these degenerate features depends on the linewidth, arising from realistic measurement conditions. Furthermore, we identify the critical quality factors q_c and q_s associated with the emergences of ZBP and RDD, respectively. The value of q_c is temperature-dependent, and we establish a suitable temperature window to ensure the visibility of single ZBP in the experiments. Whereas, q_c depends on the coupling strength rather than the temperature. Typical values for these quality factors are approximately $q_c \approx 0.93$ and $q_s \approx 0.99$. Our results suggest that the degenerate Rabi spectrum signal could serve as a hallmark for the presence of MBSs, which goes beyond the scope of differential conductance.

PACS numbers: 73.63-b, 05.40.Ca, 05.60.Gg

I. INTRODUCTION

Motivated by the promising applications in topological quantum computations [1–4], Majorana bound states (MBSs) have attracted extensive attention in both theoretical [5–12] and experimental studies [13–17]. Various realizations of the physical Majorana platforms have been proposed [5–12], with the spin-orbit coupling semiconductor nanowires proximity coupled to a superconductor emerging as a particularly popular scheme. In this platform, zero-energy MBSs are expected to reside at the ends of the nanowire. [5, 6]. Experiments are designed to validate the existence of MBSs, but the evidence remains controversial. Tunneling spectroscopy in transport measurements has been explored in both single-lead (two-terminal) [7–10], and two-lead (three-terminal) configurations [11, 12]. However, the observations of the zero-bias conductance peak and its quantized value $2e^2/h$ are insufficient for conclusively identifying the presence of MBSs [18–22]. Therefore, a more powerful approach for inferring Majorana signatures involves detecting nonlocality, such as through quantum correlation [23–30], or interferometry [31, 32]. Proposed hybrid setups, where MBSs are coupled with two quantum dots, present intriguing possibilities [27–30]. Yet, realizing these schemes remain great challenges to current experiments. So that an alternative scheme which is more realizable is still in demand.

Recently, it has been suggested that the nonlocal behavior of a topological system may be assessed through a local measurement with the aid of a quantum dot (QD) at the wires's end [33, 34], as illustrated in Fig. 1. Specifically, the Majorana non-locality is characterized by a “topological quality factor q ”, defined as [33] $q = 1 - |\lambda_2|/|\lambda_1|$, where λ_1 and λ_2 represent the couplings between the two Majorana modes and the QD. The topological quality factor q can be derived from differential conductance measurements via the QD, as experimentally demonstrated in Ref. [35]. The observed zero-bias conductance peak, aligning with a high-quality factor approaching 1 ($q \rightarrow 1$), is indicative of purely topological MBSs hosted in the SC wire. In contrast, the peak splitting associated with low-quality factor ($q < 1$) suggests the presence of trivial Andreev bound states (ABSs). Notably, ABSs with partially separated Majorana states, termed quasi-MBSs (qMBSs) with $|\lambda_2| \ll |\lambda_1|$, can also exhibit high-quality factors, mimicking the signatures of spatially separated topological MBSs [36, 37]. This similarity complicates the disinction between qMBSs and topological MBSs through the proposed local measurements [33, 34]. Consequently, two fundamental questions arise: What is the critical quality factor of qMBSs that mimic the characteristics of MBSs, and what the physical mechanisms determine this critical quality factor? Addressing these issues will be instrumental for advancing current experimental demonstrations.

*Electronic address: mao@hznu.edu.cn

†Electronic address: jsjin@hznu.edu.cn

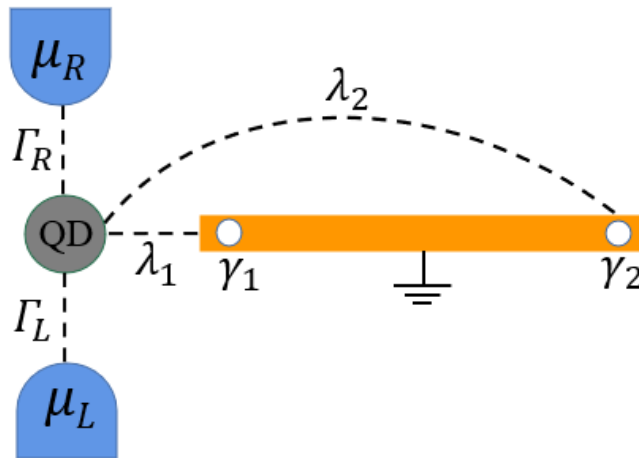


Figure 1: (Color online) Schematic diagram for the transport through the QD-wire hybrid system. The QD is contacted by the two electron reservoirs under the bias voltage ($V = \mu_L - \mu_R$) and laterally coupled to the two Majorana modes ($\hat{\gamma}_1$ and $\hat{\gamma}_2$). They are hosted in the superconducting wire with the coupling coefficients λ_1 and λ_2 , respectively.

In this paper, we will thoroughly study the quantum transport through a QD coupled with a superconducting (SC) nanowire, examining both the differential conductance and the current noise spectrum. As is well-known, shot noise stemming from nonequilibrium quantized charge current fluctuations offers profound insights into nonequilibrium quantum transport beyond the average current or the differential conductance [38–41]. In particular, the full frequency current noise spectrum can reveal the information about the intrinsic coherent dynamics of the system [42–52]. Recently, research on the Majorana-related noise in similar transport setups has garnered attention [53–57]. For instance, Smirnov demonstrated the Majorana universality of the differential shot noise at low bias voltages [55] and exhibited the universal Majorana finite-frequency features at strong coupling regimes [54]. Cao *et al.*, proposed identifying ABS-induced quantized conductance plateaus by measuring the associated differential shot noise as a function of bias voltage [57]. Here, based on both differential conductance and current noise spectrum, we first elucidate the distinct nonequilibrium transport characteristics between topological MBSs and trivial ABSs hosted in the SC wire. Subsequently, we explore how qMBSs with high-quality factors, exceeding the critical values, mimic the signatures of spatially separated topological MBSs. Importantly, we reveal the underlying mechanism governing the critical quality factors for the emergence of the zero-bias peak in differential conductance and the Rabi signal degeneracy in noise spectrum, respectively. Finally, we provide quantitative expressions for the critical quality factors, which could be instrumental for current experimental demonstrations.

The remainder of this paper is organized as follows. In Sec. II, we introduce the hybrid transport model and the employed quantum master equation approach. The related superoperators involved in current expression and the noise formula are defined in Appendix A. We present the results in Sec. III. First, we analyze the QD-wire Hamiltonian eigenspectrum in Sec. III A. Then we demonstrate the detail results for the differential conductance and the current noise spectrum in Sec. III B and Sec. III C, respectively. Finally, we give the summary in Sec. IV.

II. METHODOLOGY

A. Model description

We consider the electron transport through a quantum dot (QD) which is laterally coupled to a superconducting (SC) nanowire as schematically shown in Fig. 1. The composed Hamiltonian consists of three parts, $H_{\text{tot}} = H_B + H' + H_S$. The first part is the bath Hamiltonian of the two electron reservoirs which is given by $H_B = \sum_{\alpha} (\varepsilon_{\alpha k} + \mu_{\alpha}) \hat{c}_{\alpha k}^{\dagger} \hat{c}_{\alpha k}$, with the applied bias voltage $V = \mu_L - \mu_R$. The second part is the coupling Hamiltonian between the reservoirs and QD. It is described by the standard tunneling form,

$$H' = \sum_{\alpha=L,R} \hat{F}_{\alpha}^{\dagger} \hat{d} + \hat{d}^{\dagger} \hat{F}_{\alpha}, \quad (1)$$

where \hat{d}^\dagger (\hat{d}) is the electron creation (annihilation) operator in the QD with the assumption of a single fermionic mode, and $\hat{F}_\alpha^\dagger \equiv \sum_k t_{\alpha k} \hat{c}_{\alpha k}^\dagger$ with the tunneling coefficients $t_{\alpha k}$ and $\alpha = L, R$. Throughout this work, we adopt units of $e = \hbar = 1$ for the electron charge and the Planck constant. Introduce also the sign symbol $\sigma = \pm$ and its opposite sign $\bar{\sigma}$, for such that $\hat{d}^+ \equiv \hat{d}^\dagger$ and $\hat{d}^- \equiv \hat{d}$.

The primary interest is the QD-wire hybrid system in the third part of the composed Hamiltonian. It can be simply described by the low energy Hamiltonian [33],

$$H_S = \varepsilon_D \hat{d}^\dagger \hat{d} + i\varepsilon_M \hat{\gamma}_1 \hat{\gamma}_2 + (\lambda_1 \hat{d}^\dagger \hat{\gamma}_1 + i\lambda_2 \hat{d}^\dagger \hat{\gamma}_2 + \text{H.c.}). \quad (2)$$

Here, the first term is the Hamiltonian of the QD with the energy level ε_D . The wire hosts a pair of Majorana modes $\hat{\gamma}_1$ and $\hat{\gamma}_2$ with the coupling energy ε_M . The last term in Eq. (2) describes the coupling between the dot and two Majorana modes with the two different coupling coefficients λ_1 and λ_2 . Without loss of generality, we assume λ_1 and λ_2 to be positive real.

The quality factor is thus defined as $q = 1 - \frac{\lambda_2}{\lambda_1}$ [33]. If the wire is in the topological regime, λ_2 should be zero ($\lambda_2 \rightarrow 0$) and the quality factor approaches one ($q \rightarrow 1$). This means that there are two MBSs with the modes $\hat{\gamma}_1$ and $\hat{\gamma}_2$ located at the two ends of the wire. Otherwise ($\lambda_2 \neq 0$ and $q < 1$), the wire is in the nontopological regime where the mode $\hat{\gamma}_2$ is close to mode $\hat{\gamma}_1$. In this case, the wire bears trivial ABSs including quasi-MBSs (qMBSs) as $\hat{\gamma}_1$ and $\hat{\gamma}_2$ are partially separated with $\lambda_2 \ll \lambda_1$ [36, 37, 58, 59]. Furthermore, for the case of zero quality factor ($q = 0$ with $\lambda_2 = \lambda_1$), the two modes of $\hat{\gamma}_1$ and $\hat{\gamma}_2$ locate the same position and form a regular fermion. This leads to the disappearance of Andreev process in the dot-wire Hamiltonian of Eq. (2), as formulated explicitly in Eq. (7). In this work, our study will focus on the different characteristics of the differential conductance and current fluctuation spectrum between MBSs and ABSs hosted in SC wire. In particular, we will explore the dependence of these transport characteristics on the quality factor.

B. Quantum master equation approach

For the consideration of the weak QD-reservoir coupling [c.f. Eq. (1)], we apply the second-order quantum master equation (QME) with memory effect. It is described by the time-nonlocal QME [47, 60–62],

$$\dot{\rho}(t) = -i\mathcal{L}_S \rho(t) - \sum_{\alpha\sigma} \int_{t_0}^t d\tau [\hat{d}^{\bar{\sigma}}, \mathcal{C}_\alpha^{(\sigma)}(\mathcal{L}_S, t - \tau) \rho(\tau)], \quad (3)$$

where $\mathcal{L}_S \bullet = [H_S, \bullet]$ and

$$\mathcal{C}_\alpha^{(\sigma)}(\mathcal{L}_S, t - \tau) \bullet \equiv e^{-i\mathcal{L}_S(t-\tau)} [c_\alpha^{(\sigma)}(t - \tau) \hat{d}^\sigma \bullet - c_\alpha^{(\bar{\sigma})}(t - \tau) \bullet \hat{d}^\sigma], \quad (4)$$

with $c_\alpha^{(\sigma)}(t - \tau) = \langle \hat{F}_\alpha^\sigma(t) \hat{F}_\alpha^{\bar{\sigma}}(\tau) \rangle$ being the bath correlation function. In Eq. (3), the first term describes the intrinsic coherent dynamics of the dot-wire hybrid system. The second term depicts the non-Markovian dissipative effect of the coupled electron reservoirs.

The current through the system via the definition of $I_\alpha(t) = \langle \hat{I}_\alpha(t) \rangle$, with $\hat{I}_\alpha(t) = -d\hat{N}_\alpha(t)/dt$ and $\hat{N}_\alpha \equiv \sum_k \hat{c}_{\alpha k}^\dagger \hat{c}_{\alpha k}$, is given by [47, 50, 52]

$$I_\alpha(t) = - \sum_{\sigma u} \int_{t_0}^t d\tau \text{tr}_s [\tilde{d}^\sigma \mathcal{C}_\alpha^{(\bar{\sigma})}(\mathcal{L}_S, t - \tau) \rho(\tau)], \quad (5)$$

where $\tilde{d}^\sigma = \sigma \hat{d}^\sigma$. The stationary current can be further expressed with $\bar{I}_\alpha = [\mathcal{J}_\alpha^>(0) \bar{\rho}] = \text{tr}_s [\mathcal{J}_\alpha^<(0) \bar{\rho}]$. Here, the superoperators $\mathcal{J}_\alpha^\lessgtr$ is defined in Eq. (A1a) and $\bar{\rho}$ is the steady state of the dot-wire hybrid system which is the solution of $\dot{\rho}(t) = 0$ in Eq. (3).

The current noise spectrum, $S_{\alpha\alpha'}(\omega) = \int dt e^{i\omega t} \langle \delta \hat{I}_\alpha(t) \delta \hat{I}_{\alpha'}(0) \rangle$ with $\delta \hat{I}_\alpha(t) \equiv \hat{I}_\alpha(t) - \bar{I}_\alpha$, can be calculated via [52]

$$\begin{aligned} S_{\alpha\alpha'}(\omega) &= 2\delta_{\alpha'\alpha} \text{Re} \sum_{\sigma} \text{tr}_s [\hat{d}^{\bar{\sigma}} c_\alpha^\sigma(\omega - \mathcal{L}_S) (\hat{d}^\sigma \bar{\rho})] \\ &\quad + \text{tr}_s \left\{ \mathcal{J}_{\alpha'}^<(-\omega) \mathcal{G}(-\omega) [\mathcal{J}_\alpha^<(0) + \mathcal{W}_\alpha^<(-\omega)] \bar{\rho} \right. \\ &\quad \left. + \mathcal{J}_\alpha^>(\omega) \mathcal{G}(\omega) [\mathcal{J}_{\alpha'}^>(0) + \mathcal{W}_{\alpha'}^>(\omega)] \bar{\rho} \right\}, \end{aligned} \quad (6)$$

with the related superoperators being defined in the Appendix A. This describes the energy absorption ($\omega > 0$) and emission ($\omega < 0$) processes [48, 63, 64].

III. RESULTS

A. Eigenspectrum with parity analysis

As well-known, the Majorana modes are related to the regular fermion through the transformation of $\hat{\gamma}_1 = \hat{f} + \hat{f}^\dagger$ and $\hat{\gamma}_2 = -i(\hat{f} - \hat{f}^\dagger)$. The system Hamiltonian of Eq. (2) can be rewritten as

$$H_s = \varepsilon_D \hat{d}^\dagger \hat{d} + \varepsilon_M (\hat{f}^\dagger \hat{f} - \frac{1}{2}) + (\lambda_1 + \lambda_2) \hat{f}^\dagger \hat{d} + \text{H.c.}] + [(\lambda_1 - \lambda_2) \hat{f} \hat{d} + \text{H.c.}]. \quad (7)$$

The last two terms describe the normal tunneling and Andreev reflection processes, respectively. In the Fock states basis $\{|n_D n_M\rangle = |01\rangle, |10\rangle, |00\rangle, |11\rangle\}$, associated with $\hat{n}_D = \hat{d}^\dagger \hat{d}$ and $\hat{n}_M = \hat{f}^\dagger \hat{f}$, Eq. (7) is block diagonal,

$$H_s = \begin{pmatrix} H_- & 0 \\ 0 & H_+ \end{pmatrix}, \quad (8)$$

in the odd-parity ($p = -1$) and even-parity ($p = +1$) subspaces, with

$$H_- = \begin{pmatrix} \varepsilon_M & \lambda_1 + \lambda_2 \\ \lambda_1 + \lambda_2 & \varepsilon_D \end{pmatrix}, \quad (9a)$$

$$H_+ = \begin{pmatrix} 0 & \lambda_1 - \lambda_2 \\ \lambda_1 - \lambda_2 & \varepsilon_D + \varepsilon_M \end{pmatrix}. \quad (9b)$$

Apparently, there are intrinsic coherent Rabi oscillations in the odd and even parity subspaces which are closely related to the Majorana qubit readout [65–68]. The corresponding parity-dependent Rabi-frequency reads

$$\Delta_p = \sqrt{(\varepsilon_D + p\varepsilon_M)^2 + 4(\lambda_1 - p\lambda_2)^2}. \quad (10)$$

As known, the noise spectrum, Eq. (6), exhibits some obvious characteristics at Rabi frequency Δ_p . For instance, it has been demonstrated that a dip feature occurs at Rabi frequency in the noise spectrum in both serial and parallel coherent coupled double dots [50, 69–71]. Hence, we could expect that the parity-dependent Rabi signals at $\omega \simeq \pm\Delta_p$, via Eq. (10) with $p = \pm$, should emerge in the current noise spectrum.

On the other hand, the conductance peaks appear whenever the Fermi surface of the electrode is on resonance with the allowed transitions between the ground state and an excited state with the opposite parity [33]. The resulting peak positions are expressed in descending order as

$$\begin{aligned} E_1 &= \frac{1}{2}(\Delta_+ + \Delta_-), & E_2 &= \frac{1}{2}(-\Delta_+ + \Delta_-), \\ E_3 &= \frac{1}{2}(\Delta_+ - \Delta_-), & E_4 &= -\frac{1}{2}(\Delta_+ + \Delta_-). \end{aligned} \quad (11)$$

From Eqs. (10) and (11), it is easy to find that the zero-bias peak (ZBP) occurs at $\mu_L = V/2 = E_2 = E_3 = 0$, satisfying the condition of $\Delta_+ = \Delta_-$ that can be recast in terms of

$$\varepsilon_D \varepsilon_M = 4\lambda_1 \lambda_2. \quad (12)$$

For the wire in the topological regime ($q = 1$ with $\lambda_2 = 0$), we can have either $\varepsilon_D = 0$ or $\varepsilon_M = 0$. In each situation, the ZBP arises in the differential conductance, while the degenerate Rabi feature occurs at $\omega = \Delta_+ = \Delta_-$ in the noise spectrum. However, the ZBP of conductance splits into a pair for the trivial ABSs in the nontopological regime ($q < 1$ with $\lambda_2 \neq 0$); see Fig. 2. The similar features occur for the degenerate Rabi signal in the noise spectrum; see Fig. 4 and remarked therein.

The above analysis would imply that either the ZBP in the conductance or the degenerate Rabi signal in the noise spectrum could be taken as a hallmark for the existence of MBSs in SC wire. However, for the realistic measurement setup as shown in Fig. 1, there are line broadenings and whether the degenerate features split or not depend on the linewidth.

Note that the ZBP occurs when $\Delta_+ = \Delta_-$ in which Eq. (12) holds. To elaborate the distinct characteristics between the topological MBSs and trivial ABSs, we focus on the case of $\varepsilon_D \varepsilon_M = 0$. We identify the critical quality factor q_c for the ZBP in the conductance and also that q_s for the degenerate Rabi feature in the noise spectrum. The typical values are $q_c \approx 0.93$ and $q_s \approx 0.99$. In other words, the degenerate Rabi spectrum signal would be the hallmark of MBSs, which goes beyond the scope of differential conductance.

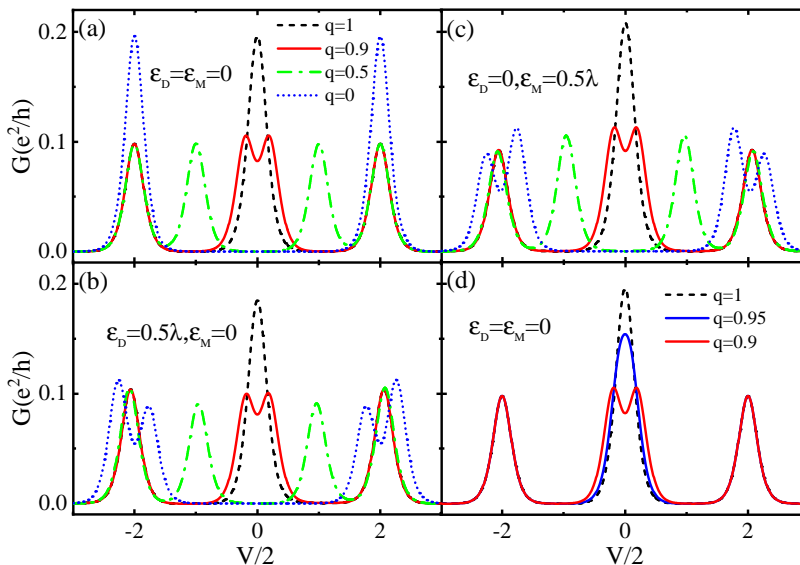


Figure 2: (Color online) The differential conductance G as a function of bias voltage V with different quality factor q . The other parameters are (in unit of λ): $k_B T = 0.1$ and $\Gamma = 0.1$.

B. The differential conductance

We first demonstrate the characteristics of differential conductance, especially the value of q_c , in the transport measurement setup of Fig. 1. In our calculations, we consider the symmetrical-lead situation, where $\mu_L = -\mu_R = V/2$ and $\Gamma_L = \Gamma_R = \Gamma/2$. Consequently, we have $G = G_L = -G_R = \frac{d\bar{I}_V}{dV}$. Furthermore, we set $\lambda_1 = \lambda = 1$ as a unit of the energy level and then $\lambda_2 = (1 - q)\lambda$. We also consider the wide bandwidth limit $W \gg \Gamma$ for the electron reservoirs. The parameters of the coupling strength Γ and the electrode temperature $k_B T$ are adopted in the weak coupling regime, where $\Gamma \lesssim k_B T$.

Figure 2 illustrates the differential conductance as a function of the bias voltage, in which the conductance peaks occur at $|\mu_\alpha| = V/2 = E_i$, with $i = 1, 2, 3, 4$. As demonstrated, the conductance displays three peaks for $q = 1$ (MBSs). The height of the ZBP is twice that of the other two peaks due to the overlap of two peaks ($E_2 = E_3 = 0$) at zero-bias voltage. For the wire hosting ABSs with $q < 1$, the ZBP splits ($E_2 \neq E_3 \neq 0$), leading to four peaks. For the regular local fermion with $q = 0$, two degenerate peaks appear at $E_1 = E_2$ and $E_3 = E_4$ when $\varepsilon_M = \varepsilon_D = 0$. On the contrary, for either $\varepsilon_D \neq 0$ or $\varepsilon_M \neq 0$, the degenerate peaks split, resulting in four peaks as displayed in Fig. 2(b) and Fig. 2(c). The heights of these four peaks are different, due to the nonsymmetric tunneling channels with $\varepsilon_M \neq \varepsilon_D$.

So far, we have understood that the key to distinguish ABSs from MBSs based on the conductance characteristics lies in observing whether the ZBP splits. Looking at Fig. 2(a)-(c), the ZBP displays the certain broadening that completely originates from the dissipative effect of the contacted electron reservoirs on the QD-wire system. This broadening, caused by the measurement, limits the distinction efficiency between MBSs and ABSs. Thus, the ZBP in the conductance cannot be the hallmark for MBSs without considering any other physical mechanisms. For example, we plot the differential conductance for a high-quality factor $q = 0.95$ (qMBSs) in Fig. 2(d). It indicates that the qMBSs indeed mimic the ZBP signature of topological MBSs, as demonstrated in previous work [36, 37].

Now we will explore the critical quality factor q_c of qMBSs that mimics the ZBP characteristic of MBSs. To that end, we provide an analytical expression using $\varepsilon_D = \varepsilon_M = 0$ as an example. The resulting differential conductance is given by

$$G(V) = \frac{\Gamma\beta}{2^7} \left(\text{sech}^2[\beta(V/4 - \lambda_1)] + \text{sech}^2[(V/4 + \lambda_1)] \right. \\ \left. + \text{sech}^2[\beta(V/4 - \lambda_2)] + \text{sech}^2[\beta(V/4 + \lambda_2)] \right), \quad (13)$$

where we have set $\lambda_1 = \lambda$ and $\lambda_2 = (1 - q)\lambda$. Obviously, the conductance in Eq. (13) indicates that the peaks arise at the bias voltage of $V/2 = E_1 = 2\lambda_1 = -E_4$ and $V/2 = E_2 = 2\lambda_2 = -E_3$, which are consistent with those given by Eq. (11). Moreover, the height of the peaks is affected by both the coupling strength and temperature, whereas the width of the peaks is solely determined by the temperature. From Eq. (13), it is easy to obtain the half-width of the

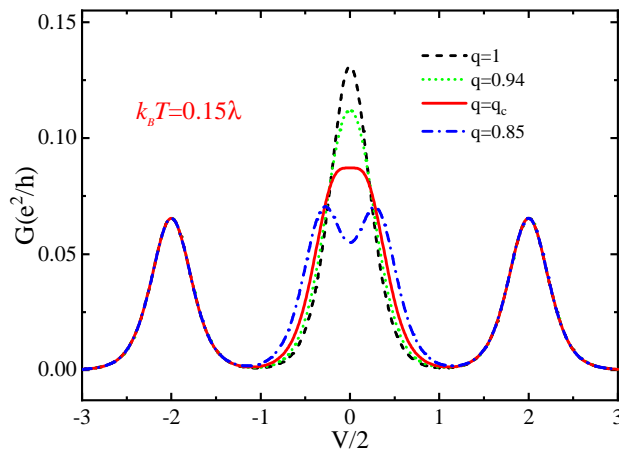


Figure 3: (Color online) The differential conductance G as a function of bias voltage V with different quality factor (q) for the demonstration of the critical quality factor q_c . For the parameters used here, $q_c \approx 0.934$. The other parameters are (in unit of λ): $k_B T = 0.15$, $\varepsilon_D = \varepsilon_M = 0$ and $\Gamma = 0.1$.

peaks as

$$\Gamma_d = 2 \ln(1 + \sqrt{2}) k_B T \approx 1.763 k_B T. \quad (14)$$

As mentioned above, the ZBP at $E_2 = E_3 = 0$ for $q = 1$ should symmetrically split into two peaks at finite values of E_2 and $E_3 = -E_2$ for $q < 1$ (ABSs), as illustrated in Fig. 2 with the example of $q = 0.9$. This implies the existence of a critical quality factor q_c , which corresponds to an inflection point in the differential conductance at $V = 0$. Based on Eq. (13), one then easily gets the critical quality factor as

$$q_c = 1 - \ln(2 + \sqrt{3}) \frac{k_B T}{2\lambda} \approx 1 - 0.66 \frac{k_B T}{\lambda}. \quad (15)$$

This suggests that we can only distinguish the conductance features between $q > q_c$ and $q < q_c$. The former displays ZBP and the latter exhibits ZBP splitting, as numerically illustrated in Fig. 3. Such a result could explain why the partially separated of qMBSs with high-quality factor ($q > q_c$ with $\lambda_2 \ll \lambda_1$) mimic the characteristics of MBSs ($q = 1$) [36, 37]. Therefore, we cannot distinguish qMBSs from spatially separated topological MBSs based on the characteristics of differential conductance.

Note that the obtained q_c in Eq. (15) is actually applicable to the cases where $\varepsilon_M = 0$ or $\varepsilon_D = 0$, and even very small values of $\varepsilon_M, \varepsilon_D \ll \lambda$. However, considering the actual situation in experiments, it is preferable to tune the energy level of the dot as $\varepsilon_D \rightarrow 0$, since the coupling energy (ε_M) of Majorana modes is determined by the length of the wire.

Furthermore, we emphasize that the present work focuses on the weak system-reservoir coupling regime, where $\Gamma \lesssim k_B T$. However, the ZBP will be smoothed by increasing the temperature, with its half-width broadening given by Eq. (14). Considering the measurement visibility of a single ZBP, the distance between the ZBP and its nearby symmetric peaks should be greater than the broadening width, i.e., $|E_1| = |E_4| > 2\Gamma_d$. This results in $k_B T < \frac{\lambda}{2 \ln(1 + \sqrt{2})}$. Therefore, we identify the valid temperature window as

$$\Gamma \lesssim k_B T < \frac{\lambda}{2 \ln(1 + \sqrt{2})}, \quad (16)$$

for the experimental observation of the ZBP.

C. The noise spectrum

We are now in the position to demonstrate the characteristics in the current noise spectrum, with a particular focus on exploring the value of q_s . As known, the noise spectrum contains the information beyond the conductance [38–41]. The differential conductance reflects the energy transition (or structure) information of the QD-wire system as illustrated above. In contrast, the current noise spectrum is related to not only the energy transitions but also the intrinsic coherent dynamics of the system [42–52]. For the former, it is manifested as the non-Markovian quasi-steps

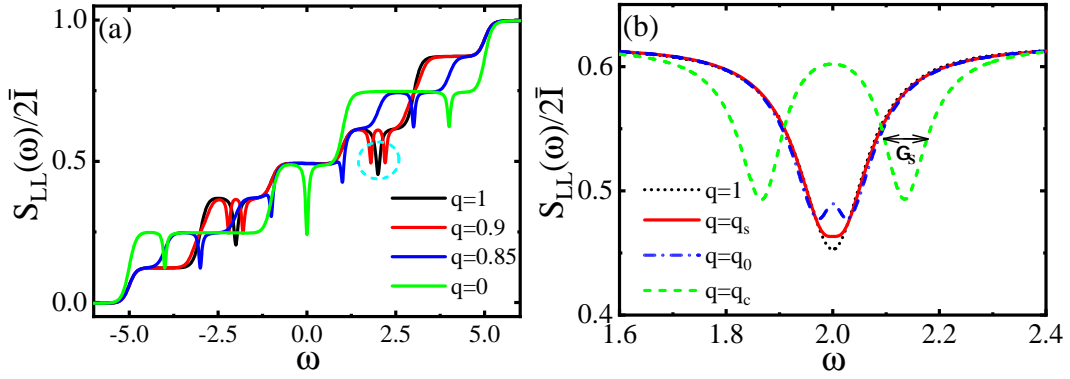


Figure 4: (Color online) The auto-correlation current noise spectrum of the left-lead, $S_{LL}(\omega)$, with different quality factors, for (a) the whole frequency-regime and (b) the regime around the Rabi frequencies. The value of $q_c \approx 0.934$ is the same as in Fig. 2. Here $q_0 \approx 0.9885$ and $q_s \approx 0.994$. The other parameters are (in unit of λ) $\varepsilon_M = \varepsilon_D = 0$, $\Gamma = 0.1$, $k_B T = 0.1$, and $V = 6$.

at resonance frequencies, $\pm|\mu_\alpha - E_i|$, as depicted in Fig. 4 (a). This feature arises from the non-Markovian dynamics of the electrons in α -electrode tunneling into and out of the system, accompanied by energy absorption ($\omega > 0$) and emission ($\omega < 0$), respectively. The corresponding differential characteristics ($\frac{dS_{LL}(\omega)}{d\omega}$), display peaks at $\pm|\mu_\alpha - E_i|$, which resemble those observed in the differential conductance [72].

Of particular interest is the characteristic of the intrinsic coherent dynamics in the noise spectrum. It exhibits the coherent Rabi dip signal at $\omega \approx \pm\Delta_p$, as illustrated in Fig. 4 (a). This attribute is derived from the propagator $\mathcal{G}(\omega)$ [c.f. Eq. (A2)] in the second and third terms of Eq. (6). Akin to the conductance, the noise spectrum displays the similar feature for either $\varepsilon_M = 0$ or $\varepsilon_D = 0$. For simplicity and without loss of generality, we use $\varepsilon_M = \varepsilon_D = 0$ as an illustrative example in subsequent discussions.

As shown in Fig. 4 (a), $S_{LL}(\omega)$ displays a deep Rabi dip, which we refer to as Rabi dips degeneracy (RDD), at $\Delta_+ = \Delta_-$ for $q = 1$ (MBSs). The RDD is separated into two dips at Δ_+ and $\Delta_- \neq \Delta_+$, respectively, for $0 < q < 1$ (ABSs). When $q = 0$ (i.e., $\lambda_1 = \lambda_2$), the Rabi signal at Δ_+ vanishes for the disappearance of the Andreev reflection processes; see Eq. (7). The resulting noise spectrum displays only one dip at $\Delta_- = 2\sqrt{2}\lambda$ in the high frequency regime.

Therefore, the crux to distinguish ABSs from MBSs in the noise spectrum is to observe whether the RDD is split, as indicated by the dashed circle in Fig. 4 (a). Analogous to the ZBP feature in differential conductance, the Rabi dip in the noise spectrum exhibits a certain broadening that may hinder the efficiency of distinguishing between MBSs and ABSs. Given the complexity of the analytical results, our discussions are primarily based on the numerical calculations. Our findings indicate that, unlike the conductance, the broadening (Γ_s) of the Rabi dip in the noise spectrum is predominantly determined by the coupling strength (Γ) rather than the temperature ($k_B T$). Specifically, we observe that $\Gamma_s \approx 4\Gamma/5$, as denoted by the double arrow in Fig. 4 (b). The critical quality factor q_s is consequently obtained as

$$q_s \approx 1 - \frac{5\Gamma_s}{72\lambda} \approx 1 - \frac{\Gamma}{18\lambda}. \quad (17)$$

It is higher than that of the Lorentz counterpart:

$$q_0 = 1 - \frac{\Gamma_s}{4\sqrt{3}\lambda} \approx 1 - \frac{\Gamma}{5\sqrt{3}\lambda}. \quad (18)$$

Figure 4 (b) illustrates that for $q > q_s$, RDD is present, while for $q < q_s$, RDD is split. Intriguingly, in the regime of weak coupling and low temperature determined by Eq. (16), the critical quality factor q_s is typically higher than 0.99. For the parameters used in Fig. 4 with $\Gamma = 0.1\lambda$, we calculate $q_s \approx 0.994$. By further reducing the coupling strength Γ , q_s approaches 1. In this sense, the RDD signal in the noise spectrum emerges as a potential hallmark for the existence of MBSs in SC wire. This suggests that by analyzing the noise spectrum, one may be able to identify the presence of MBSs with high accuracy.

IV. SUMMARY

In summary, we have thoroughly studied the differential conductance and the noise spectrum of the transport current through the quantum dot coupled with a SC wire. The study is based on the quantum master equation

approach for weak system-reservoir coupling regime ($\Gamma \lesssim k_B T$). We analyzed the distinct nonequilibrium transport characteristics between the topological MBSs and trival ABSs hosted in the SC wire. For the SC nanowire hosting topological MBSs with the topological quality factor $q = 1$, we demonstrated the degenerate characteristics: the zero-bias peak (ZBP) in differential conductance and the Rabi dips degeneracy (RDD) in noise spectrum. In contrast, for the SC nanowire bearing ABSs with $q < 1$, whether the degenerate features split or not depend on the linewidth, due to the line broadenings inherent in realistic measurement setups. Furthermore, we identified the critical quality factors q_c and q_s for the emergences of the ZBP in differential conductance and the RDD in current noise spectrum, respectively.

For the differential conductance, we derived an analytical expression for q_c . It enable us to distinguish the conductance features between $q > q_c$ and $q < q_c$, exhibiting a ZBP and ZBP splitting. The resulted q_c depends on the temperature of the electron reservoirs. In addition, we identified a valid temperature window for experimental measurements to ensure the visibility of a single ZBP

For the current noise spectrum, we numerically validated the critical quality factor q_s for RDD. Notably, q_s is determined by the system-reservoir coupling strength rather than the temperature, and surprisingly approaches one ($q_s \rightarrow 1$) in the considered weak system-reservoir coupling regime. Thus, beyond the scope of differential conductance, the RDD signal in the noise spectrum would serve as a hallmark for the existence of MBSs in SC wires. We anticipate that our findings will provide valuable insights for ongoing experimental demonstrations.

Acknowledgments

We acknowledge helpful discussions Prof. YiJing Yan. The support from the Natural Science Foundation of China (Grant No. 12175052) is acknowledged.

Appendix A: Superoperators in the noise spectrum formula

The detail derivation for the noise spectrum formula Eq.(6) can refer to Ref.52. The involved superoperators in Eq.(6) read,

$$\mathcal{J}_\alpha^>(\omega)\hat{O} \equiv -\sum_\sigma \tilde{d}^{\bar{\sigma}} [\mathcal{C}_\alpha^{(\sigma)}(\omega - \mathcal{L}_s)\hat{O}], \quad (\text{A1a})$$

$$\mathcal{J}_\alpha^<(\omega)\hat{O} \equiv -\sum_\sigma [\mathcal{C}_\alpha^{(\sigma)}(\omega - \mathcal{L}_s)\hat{O}] \tilde{d}^{\bar{\sigma}}, \quad (\text{A1b})$$

$$\mathcal{W}_\alpha^>(\omega)\hat{O} \equiv \sum_\sigma [\tilde{d}^{\bar{\sigma}}, c_\alpha^\sigma(\omega - \mathcal{L}_s)(\hat{d}^\sigma \hat{O})], \quad (\text{A1c})$$

$$\mathcal{W}_\alpha^<(\omega)\hat{O} \equiv \sum_\sigma [\tilde{d}^{\bar{\sigma}}, c_\alpha^{\bar{\sigma}*}(\mathcal{L}_s - \omega)(\hat{O} \hat{d}^\sigma)], \quad (\text{A1d})$$

and the propagator is given by

$$\mathcal{G}(\omega) = [i(\mathcal{L}_s - \omega) + \Sigma(\omega)]^{-1}, \quad (\text{A2})$$

with

$$\Sigma(\omega)\hat{O} = \sum_{\alpha\sigma} [\hat{d}^{\bar{\sigma}}, \mathcal{C}_\alpha^{(\sigma)}(\omega - \mathcal{L}_s)\hat{O}]. \quad (\text{A3})$$

Here [cf. Eq. (4)]

$$\mathcal{C}_\alpha^{(\sigma)}(\omega)\hat{O} = \sum [c_\alpha^\sigma(\omega)(\hat{d}^\sigma \hat{O}) - c_\alpha^{\bar{\sigma}*}(-\omega)(\hat{O} \hat{d}^\sigma)], \quad (\text{A4})$$

with $c_\alpha^\sigma(\omega) \equiv \int_0^\infty dt e^{i\omega t} c_\alpha^\sigma(t)$. It is obtained as [50, 52, 62, 73]

$$c_\alpha^{(\pm)}(\omega) = \frac{1}{2} [\Gamma_\alpha^{(\pm)}(\mp\omega) + i\Lambda_\alpha^{(\pm)}(\mp\omega)], \quad (\text{A5})$$

where $\Gamma_\alpha^\pm(\omega) = f_\alpha^\pm(\omega)\Gamma_\alpha(\omega)$ with $f_\alpha^+(\omega)$ the Fermi-function of α -lead and $f_\alpha^-(\omega) = 1 - f_\alpha^+(\omega)$. In Eq.(A5), the real and the imaginary parts are the so-called bath interaction spectrum and *dispersion*, respectively [74]. They are

related via the Kramers-Kronig relations, $\Lambda_{\alpha}^{(\pm)}(\omega) = \mathcal{P} \int_{-\infty}^{\infty} \frac{d\omega'}{2\pi} \frac{1}{\omega \pm \omega'} \Gamma_{\alpha}^{(\pm)}(\omega')$. For the consideration of the Lorentzian-type form of the hybridization spectral density, i.e., $\Gamma_{\alpha}(\omega) = \frac{\Gamma_{\alpha} W_{\alpha}^2}{(\omega - \mu_{\alpha})^2 + W_{\alpha}^2}$, with the coupling strength Γ_{α} and the bandwidth W_{α} of lead- α , one can obtain

$$\Lambda_{\alpha}^{(\pm)}(\omega) = \frac{\Gamma_{\alpha}(\omega)}{2\pi} \left\{ \text{Re} \left[\Psi \left(\frac{1}{2} + i \frac{\beta(\omega - \mu_{\alpha})}{2\pi} \right) \right] - \Psi \left(\frac{1}{2} + \frac{\beta W_{\alpha}}{2\pi} \right) \mp \pi \frac{\omega - \mu_{\alpha}}{W_{\alpha}} \right\}, \quad (\text{A6})$$

where \mathcal{P} denotes the principle value of the integral, and $\Psi(x)$ is the digamma function.

-
- [1] A. Y. Kitaev, *Physics-Uspekhi* **44**, 131 (2001).
 - [2] A. Kitaev, *Annals of Physics* **303**, 2 (2003).
 - [3] C. Nayak, S. H. Simon, A. Stern, M. Freedman, and S. Das Sarma, *Rev. Mod. Phys.* **80**, 1083 (2008).
 - [4] M. Leijnse and K. Flensberg, *Phys. Rev. Lett.* **107**, 210502 (2011).
 - [5] R. M. Lutchyn, J. D. Sau, and S. Das Sarma, *Phys. Rev. Lett.* **105**, 077001 (2010).
 - [6] Y. Oreg, G. Refael, and F. von Oppen, *Phys. Rev. Lett.* **105**, 177002 (2010).
 - [7] K. Flensberg, *Phys. Rev. B* **82**, 180516 (2010).
 - [8] S. Das Sarma, A. Nag, and J. D. Sau, *Phys. Rev. B* **94**, 035143 (2016).
 - [9] C. Moore, T. D. Stanescu, and S. Tewari, *Phys. Rev. B* **97**, 165302 (2018).
 - [10] K. T. Law, P. A. Lee, and T. K. Ng, *Phys. Rev. Lett.* **103**, 237001 (2009).
 - [11] J. Danon et al., *Phys. Rev. Lett.* **124**, 036801 (2020).
 - [12] G. C. Ménard et al., *Phys. Rev. Lett.* **124**, 036802 (2020).
 - [13] V. Mourik et al., *Science* **336**, 1003 (2012).
 - [14] M. T. Deng et al., *Nano Lett.* **12**, 6414 (2012).
 - [15] A. Das et al., *Nat. Phys.* **8**, 887 (2012).
 - [16] A. D. K. Finck, D. J. Van Harlingen, P. K. Mohseni, K. Jung, and X. Li, *Phys. Rev. Lett.* **110**, 126406 (2013).
 - [17] S. M. Albrecht et al., *Nature* **531**, 206 (2016).
 - [18] C.-X. Liu, J. D. Sau, T. D. Stanescu, and S. Das Sarma, *Phys. Rev. B* **96**, 075161 (2017).
 - [19] O. A. Awoga, J. Cayao, and A. M. Black-Schaffer, *Phys. Rev. Lett.* **123**, 117001 (2019).
 - [20] J. Avila, F. Penaranda, E. Prada, P. San-Jose, and R. Aguado, *Commun. Physics* **2**, 133 (2019).
 - [21] P. San-Jose, J. Cayao, E. Prada, and R. Aguado, *Sci. Rep.* **6**, 21427 (2016).
 - [22] J. Cayao, E. Prada, P. San-Jose, and R. Aguado, *Phys. Rev. B* **91**, 024514 (2015).
 - [23] C. J. Bolech and E. Demler, *Phys. Rev. Lett.* **98**, 237002 (2007).
 - [24] J. Nilsson, A. R. Akhmerov, and C. W. J. Beenakker, *Phys. Rev. Lett.* **101**, 120403 (2008).
 - [25] L. Qin, W. Feng, and X.-Q. Li, *Chinese Physics B* **31**, 017402 (2022).
 - [26] Y. Cao, P. Wang, G. Xiong, M. Gong, and X.-Q. Li, *Phys. Rev. B* **86**, 115311 (2012).
 - [27] B. Zocher and B. Rosenow, *Phys. Rev. Lett.* **111**, 036802 (2013).
 - [28] H.-F. Lü, H.-Z. Lu, and S.-Q. Shen, *Phys. Rev. B* **90**, 195404 (2014).
 - [29] H.-F. Lü, H.-Z. Lu, and S.-Q. Shen, *Phys. Rev. B* **93**, 245418 (2016).
 - [30] W. Feng, L. Qin, and X.-Q. Li, *New Journal of Physics* **23**, 123032 (2021).
 - [31] J. D. Sau, B. Swingle, and S. Tewari, *Phys. Rev. B* **92**, 020511 (2015).
 - [32] M. Hell, K. Flensberg, and M. Leijnse, *Phys. Rev. B* **97**, 161401 (2018).
 - [33] D. J. Clarke, *Phys. Rev. B* **96**, 201109 (2017).
 - [34] E. Prada, R. Aguado, and P. San-Jose, *Phys. Rev. B* **96**, 085418 (2017).
 - [35] M.-T. Deng et al., *Phys. Rev. B* **98**, 085125 (2018).
 - [36] C.-X. Liu, J. D. Sau, and S. Das Sarma, *Phys. Rev. B* **97**, 214502 (2018).
 - [37] A. Vuik, B. Nijholt, A. R. Akhmerov, and M. Wimmer, *SciPost Phys.* **7**, 61 (2019).
 - [38] S. Hershfield, *Phys. Rev. B* **46**, 7061 (1992).
 - [39] Y. M. Blanter and M. Büttiker, *Phys. Rep.* **336**, 1 (2000).
 - [40] I. Imry, *Introduction to Mesoscopic Physics*, Oxford university press, 2002.
 - [41] *Quantum Noise in Mesoscopic Physics*, Kluwer, Dordrecht, 2003, edited by Y. V. Nazarov.
 - [42] O. Entin-Wohlman, Y. Imry, S. A. Gurvitz, and A. Aharony, *Phys. Rev. B* **75**, 193308 (2007).
 - [43] X. Q. Li, P. Cui, and Y. J. Yan, *Phys. Rev. Lett.* **94**, 066803 (2005).
 - [44] S. D. Barrett and T. M. Stace, *Phys. Rev. Lett.* **96**, 017405 (2006).
 - [45] J. Wabnig, B. W. Lovett, J. H. Jefferson, and G. A. D. Briggs, *Phys. Rev. Lett.* **102**, 016802 (2009).
 - [46] J. S. Jin, M. Marthaler, P.-Q. Jin, D. Golubev, and G. Schön, *New J. Phys.* **15**, 025044 (2013).
 - [47] J. S. Jin, X. Q. Li, M. Luo, and Y. J. Yan, *J. Appl. Phys.* **109**, 053704 (2011).

- [48] E. A. Rothstein, O. Entin-Wohlman, and A. Aharony, *Phys. Rev. B* **79**, 075307 (2009).
- [49] P.-Y. Yang, C.-Y. Lin, and W.-M. Zhang, *Phys. Rev. B* **89**, 115411 (2014).
- [50] P. Shi, M. Hu, Y. Ying, and J. Jin, *AIP ADVANCES* **6**, 095002 (2016).
- [51] J. S. Jin, *Phys. Rev. B* **101**, 235144 (2020).
- [52] Y. Xu, J. Jin, S. Wang, and Y. Yan, *Phys. Rev. E* **106**, 064130 (2022).
- [53] D. E. Liu, M. Cheng, and R. M. Lutchyn, *Phys. Rev. B* **91**, 081405 (2015).
- [54] S. Smirnov, *Phys. Rev. B* **99**, 165427 (2019).
- [55] S. Smirnov, *Phys. Rev. B* **105**, 205430 (2022).
- [56] G.-H. Feng and H.-H. Zhang, *Phys. Rev. B* **105**, 035148 (2022).
- [57] Z. Cao et al., *Phys. Rev. B* **108**, L121407 (2023).
- [58] C.-K. Chiu and S. Das Sarma, *Phys. Rev. B* **99**, 035312 (2019).
- [59] C. Moore, C. Zeng, T. D. Stanescu, and S. Tewari, *Phys. Rev. B* **98**, 155314 (2018).
- [60] Y. J. Yan and R. X. Xu, *Annu. Rev. Phys. Chem.* **56**, 187 (2005).
- [61] Y. Makhlin, G. Schön, and A. Shnirman, *Rev. Mod. Phys.* **73**, 357 (2001).
- [62] J. S. Jin, C. Karlewski, and M. Marthaler, *New J. Phys.* **18**, 083038 (2016).
- [63] H.-A. Engel and D. Loss, *Phys. Rev. Lett.* **93**, 136602 (2004).
- [64] J. S. Jin, S. K. Wang, X. Zheng, and Y. J. Yan, *J. Chem. Phys.* **142**, 234108 (2015).
- [65] K. Gharavi, D. Hoving, and J. Baugh, *Phys. Rev. B* **94**, 155417 (2016).
- [66] M. I. K. Munk, J. Schulenburg, R. Egger, and K. Flensberg, *Phys. Rev. Res.* **2**, 033254 (2020).
- [67] J. F. Steiner and F. von Oppen, *Phys. Rev. Res.* **2**, 033255 (2020).
- [68] A. Khindanov, D. Pikulin, and T. Karzig, *SciPost Phys.* **10**, 127 (2021).
- [69] J. Y. Luo, X. Q. Li, and Y. J. Yan, *Phys. Rev. B* **76**, 085325 (2007).
- [70] B. Dong, X. L. Lei, and N. J. M. Horing, *J. Appl. Phys.* **104**, 033532 (2008).
- [71] D. Marcos, C. Emary, T. Brandes, and R. Aguado, *Phys. Rev. B* **83**, 125426 (2011).
- [72] H. Mao, J. Jin, S. Wang, and Y. Yan, *The Journal of Chemical Physics* **155**, 014104 (2021).
- [73] J. S. Jin, J. Li, Y. Liu, X.-Q. Li, and Y. J. Yan, *J. Chem. Phys.* **140**, 244111 (2014).
- [74] R. X. Xu and Y. J. Yan, *J. Chem. Phys.* **116**, 9196 (2002).